analytical chemistry

pubs.acs.org/ac Article

Multigas Sensing Technique Based on Quartz Crystal Tuning Fork-Enhanced Laser Spectroscopy

Linguang Xu, Sheng Zhou, Ningwu Liu, Minghui Zhang, Jingqiu Liang, and Jingsong Li*

Cite This: *Anal. Chem.* 2020, 92, 14153−14163 Read Online

ACCESS | Metrics & More | Article Recommendations

ABSTRACT: A compact multigas sensor system based on a single quartz crystal tuning fork (QCTF) and multifrequency synchronous modulation strategy is proposed for trace gas detection. To demonstrate the novel detection technique, three near-infrared continuous-wave (CW) distributed feedback (DFB) diode lasers with center wavelengths of near 1391, 1574, and 1653 nm and a standard 32 kHz QCTF were integrated for simultaneous detection of H_2O, CO_2, and CH_4, respectively. Wavelength modulation spectroscopy with second harmonic detection (WMS-2*f*) was selected for enhancing sensitivity. Design of the sensor configuration and primary performance between the traditional single-frequency modulation and the proposed tri-frequency modulation were experimentally investigated and compared in detail. The results indicate that the proposed sensing technique has significant advantages of cost effectiveness, portability, and ease-of-use, and detection limits of 1.4, 353, and 3.1 ppm for simultaneously measuring H_2O, CO_2, and CH_4, respectively, are obtained, corresponding to the normalized noise equivalent absorption (NNEA) coefficients of 2.65×10^{-10}, 8.09×10^{-10}, and 8.28×10^{-10} cm^{-1} W/$\sqrt{Hz}$, respectively. Moreover, the use of an erbium-doped fiber amplifier (EDFA) has been demonstrated as an effective method for sensitivity enhancement.

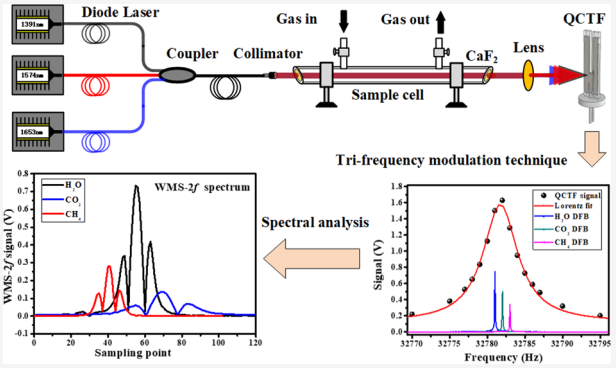

Laser spectroscopy-based trace gas detection techniques, such as commonly used direct absorption spectroscopy (DAS) and photoacoustic spectroscopy (PAS),[1−4] are widely implemented in atmospheric monitoring, industrial process control, aerospace, and medical technology fields.[5−8] With the development of various spectroscopy techniques, the detector as a key element of a spectroscopy system is also updated. In 2002, Kosterev et al.[9] first reported a quartz crystal tuning fork (QCTF) as a photoacoustic signal detector in PAS, which was known as quartz-enhanced photoacoustic spectroscopy (QEPAS), instead of a traditional microphone. Since then, the quartz tuning fork as a new type of sound transducer has been widely employed and aroused a strong research interest in QEPAS-based gas sensing.[10−13] On the other hand, the mini QCTF is investigated as an optical detector for trace gas and volatile organic compound (VOC) detection in standoff laser spectroscopy[14−16] and wavelength modulation spectroscopy (WMS).[17,18] Trace gas detection systems based on the QCTF are widely developed mainly due to the small size, low cost, low power consumption, high precision and high quality-factor (*Q* factor), long stability, and fully digital frequency output signal of the QCTF.[19−21]

In practical applications, the ability to detect multiple components simultaneously for a gas sensor is of great importance apart from the requirement of economic cost. For example, the correlations between multicomponent trace gases are very useful for us to accurately identify atmospheric pollution sources[22] and physical symptoms[23] in the fields of environmental monitoring and human respiratory diagnosis, respectively. Due to the molecular properties of the analytes of interest, their absorption lines (especially for strong transition lines suitable for high sensitivity detection) are clearly separated and thus could not be easily covered by a single tunable laser source. With the dramatic improvement in novel light sources and optical or acoustic detectors, as well as signal recovery electronics, various sensing strategies based on the tunable laser absorption spectroscopy technique (TDLAS) have been developed for multigas detection, typically three or more gas species, such as the multiple laser light source scheme[24,25] and the time or frequency division multiplex detection method.[26,27] Over the past decades, quantum cascade lasers (QCLs) have been proven as attractive and promising light sources for developing gas sensors. The emitted wavelength within ten wavenumbers is usually

Received: July 30, 2020
Accepted: September 21, 2020
Published: September 21, 2020

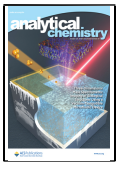

https://dx.doi.org/10.1021/acs.analchem.0c03233
Anal. Chem. 2020, 92, 14153−14163

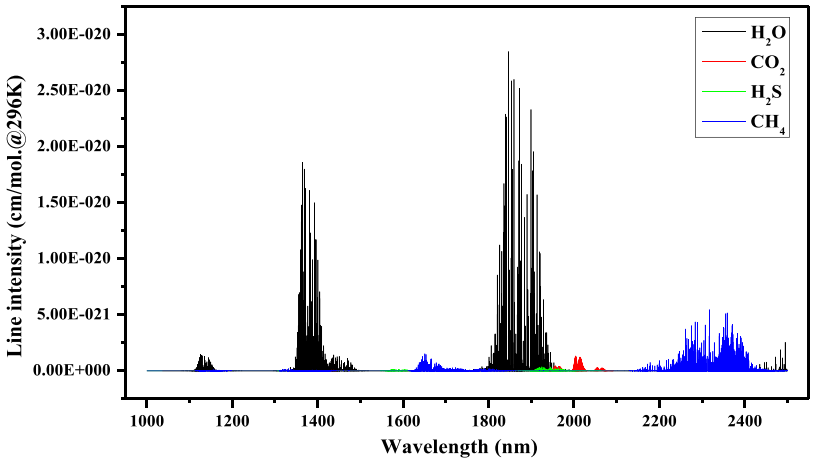

Figure 1. Absorption lines simulated based on the HITRAN database.

obtained by either changing the injected current or the temperature of the gain element. However, some typical analytes of interest are discretely distributed over the mid-infrared range and cannot be covered by a single QCL, therefore, multiple QCL lasers are also necessary.[28−30] Although a QCL with an external cavity (EC-QCL) scheme can already cover a spectral range of >400 cm^{-1}[31] and has been demonstrated for simultaneous detection of multiple atmospheric species and VOCs,[32−34] it is rather unsuited for development of field-deployable compact gas sensors and still remains expensive. In comparison, near-infrared tunable distributed feedback (DFB) diode lasers were widely recognized as suitable light sources for developing optical spectroscopy gas sensors due to their long lifetime, compact size, low cost and low power consumption, wavelength tunability, high spectral quality, and reliability.

In this article, a compact multigas sensor system based on a single QCTF and multifrequency synchronous modulation strategy is proposed for multiple trace gas detection. To demonstrate this technique, three near-infrared continuous-wave (CW) DFB diode lasers with center wavelengths of near 1391, 1574, and 1653 nm and a standard 32 kHz QCTF were integrated for simultaneous detection of H_2O, CO_2, and CH_4, respectively. Wavelength modulation spectroscopy with second harmonic detection (WMS-2*f*) was selected for enhancing sensitivity. Design of the sensor configuration and primary performance between single-frequency modulation and tri-frequency modulation were experimentally investigated and compared in detail. Potential methods for sensitivity enhancement are also demonstrated and discussed.

EXPERIMENTAL DETAILS

Absorption Line Selection. Methane (CH_4) and carbon dioxide (CO_2) are two important greenhouse gases that play an important role in climate change and global warming.[35,36] Hydrogen sulfide (H_2S) is a colorless, flammable, explosive, and highly toxic natural gas component.[37−39] H_2O is an important molecule with high content in atmospheric components. Therefore, CH_4, CO_2, H_2S, and H_2O were initially selected as the target species to demonstrate the reported sensor technique due to their important influence in the atmospheric environment. Figure 1 shows the absorption line intensity (@296K) of each molecule in the near-infrared band (1−2.5 μm) taken from the HITRAN database.[40] Three near-infrared DFB diode lasers with center emitting wavelengths near 1391, 1574, and 1653 nm are initially selected as the excitation light source for evaluating the multigas sensing system. Table 1 summarizes the selected line parameters of the four target molecules. Note that the H_2O absorption line near 1391.67 nm and CH_4 absorption line near 1653.72 nm are multiple merge states, which include two and three lines, respectively, and are thus very hard to be distinguished even under the Doppler broadening limit. Due to the impact of COVID-19, the hydrogen sulfide standard gas sample is insufficient; thus, the related experiments are not provided here. Detailed carbon dioxide measurements were made using the same laser of hydrogen sulfide. Obviously, all of the spectral lines selected in the NIR region are much weaker than the optimal transitions in the MIR spectral region. However, the absolute sensitivity is not the greatest concern in this work.

Table 1. Line Intensity Parameters for the Selected Four Species of Interest

species	wavelength (nm)	wavenumber (cm^{-1})	line intensity (cm/mol)
H_2O	1391.67276	7185.59728	5.931×10^{-22}
	1391.6729	7185.59655	1.977×10^{-22}
CO_2	1574.03395	6353.10312	1.134×10^{-23}
H_2S	1573.93068	6353.51996	4.36×10^{-23}
CH_4	1653.72254	6046.96359	1.455×10^{-21}
	1653.72582	6046.9516	9.277×10^{-22}
	1653.7283	6046.9425	7.877×10^{-22}

DFB Diode Laser Characteristics. Generally, the emission wavelength of a near-infrared DFB diode laser can be achieved by scanning its operating temperature or driving voltage. To accurately control the lasers and to achieve covering the absorption spectra of the four target analytes, the characteristics of the selected three DFB lasers used in this experiment were first tested. For this experiment, the absolute wavelength versus driving voltage was recorded with a high precision wavemeter (HighFinesse GmbH, WS6−200) at a fixed operating temperature. For example, the relationship between the laser wavelength and driving voltage at different temperatures was recorded, as shown in Figure 2. According to these calibration results, the laser operating temperatures of 33, 30, and 30 °C were used for targeting the H_2O absorption line near 1391.67 nm, CO_2 absorption line near 1574.03 nm, and CH_4 absorption line near 1653.72 nm, respectively. The

https://dx.doi.org/10.1021/acs.analchem.0c03233
Anal. Chem. 2020, 92, 14153−14163

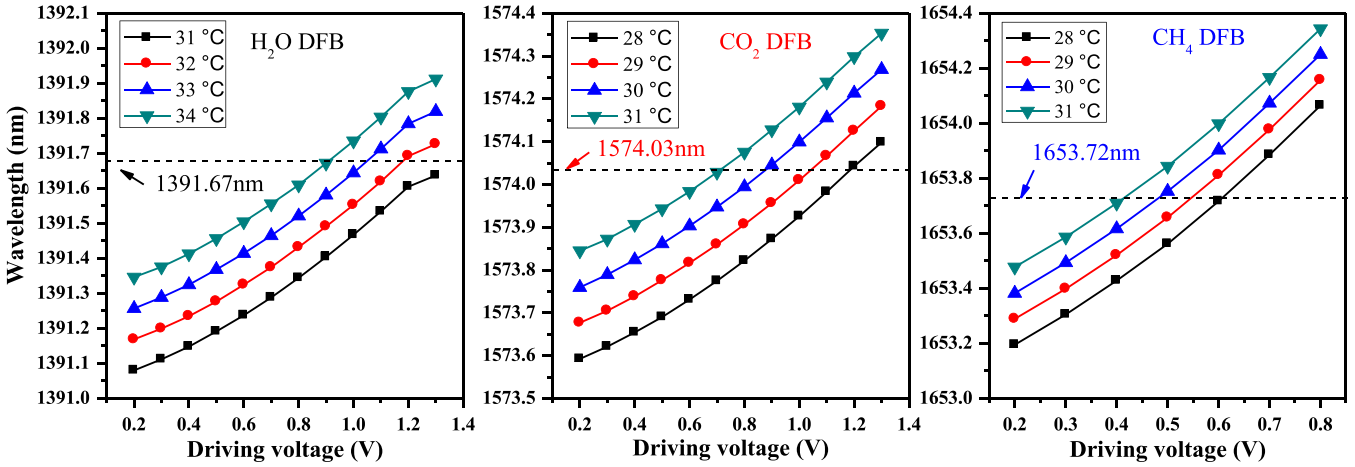

Figure 2. Emission wavelength of the diode laser as a function of the TEC temperature and driving voltage.

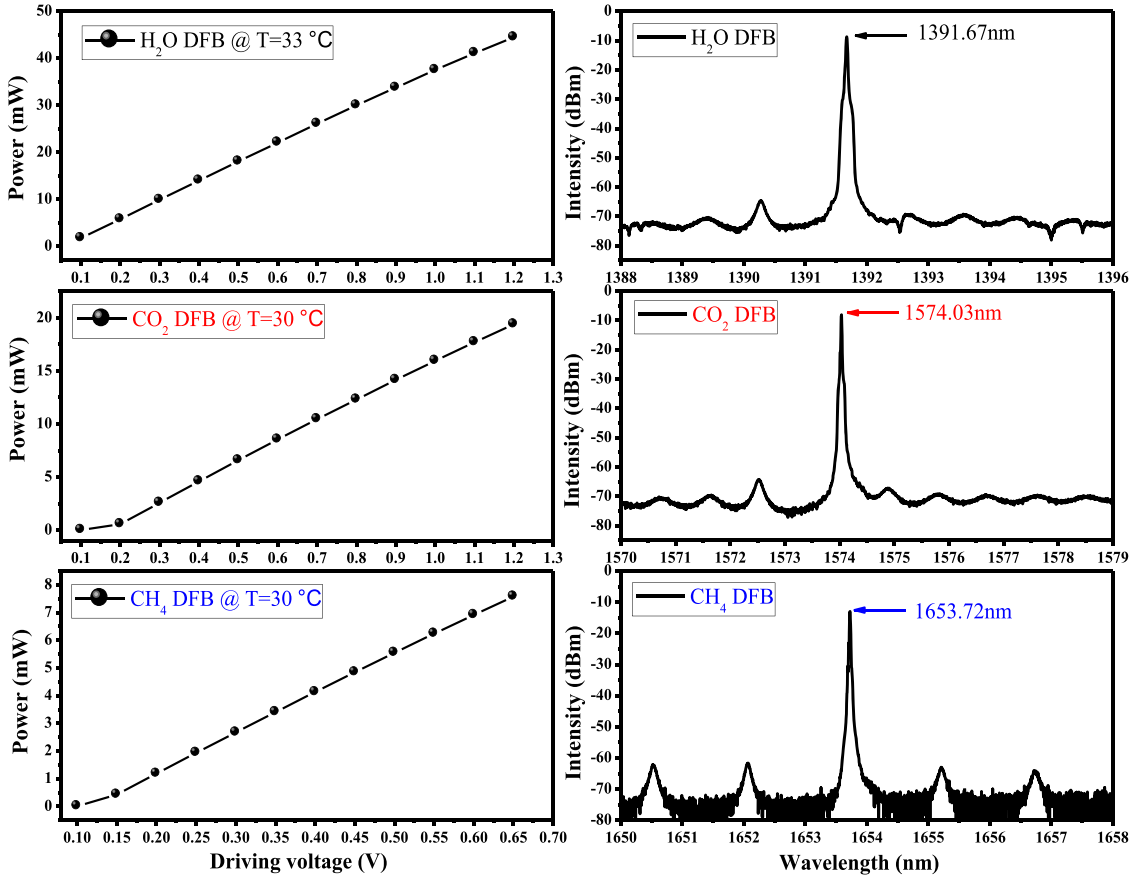

Figure 3. Output power versus driving voltage (left panel) and the emission spectra of the three diode lasers (right panel).

relationship between the laser output power and driving voltage at the selected operating temperature is presented in Figure 3 (left panel).

In this condition, the maximum output power of 44.41 mW for the H_2O DFB diode laser, 19.39 mW for the CO_2 DFB diode laser, and 7.58 mW for the CH_4 DFB diode laser, can be obtained. The laser powers are measured at the laser light outlet using a handheld optical power meter (EXFO FPM-300). The emission spectrum for each DFB laser was also investigated and measured by an optical spectrum analyzer (OSA, Yokogawa AQ6370C), as demonstrated in Figure 3 (right panel). The corresponding side mode suppression ratios (SMSR) were 56, 56, and 48 dB, respectively.

Sensor System Configuration. The proposed multigas sensor system configuration is shown in Figure 4. Laser beams from three fiber-coupled DFB diode lasers were directly coupled into a 3 × 1 fiber coupler and collimated by a collimator before their entry into the gas cell (with two CaF_2 windows and an optical path of 50 cm). After exiting the gas sample cell, the integrated laser beams were focused by a CaF_2 lens and were detected by a single QCTF-based detector for spectral signal measurements. Similar to the photoelectric effect of semiconductor detectors, we utilize the piezoelectric

https://dx.doi.org/10.1021/acs.analchem.0c03233
Anal. Chem. 2020, 92, 14153−14163

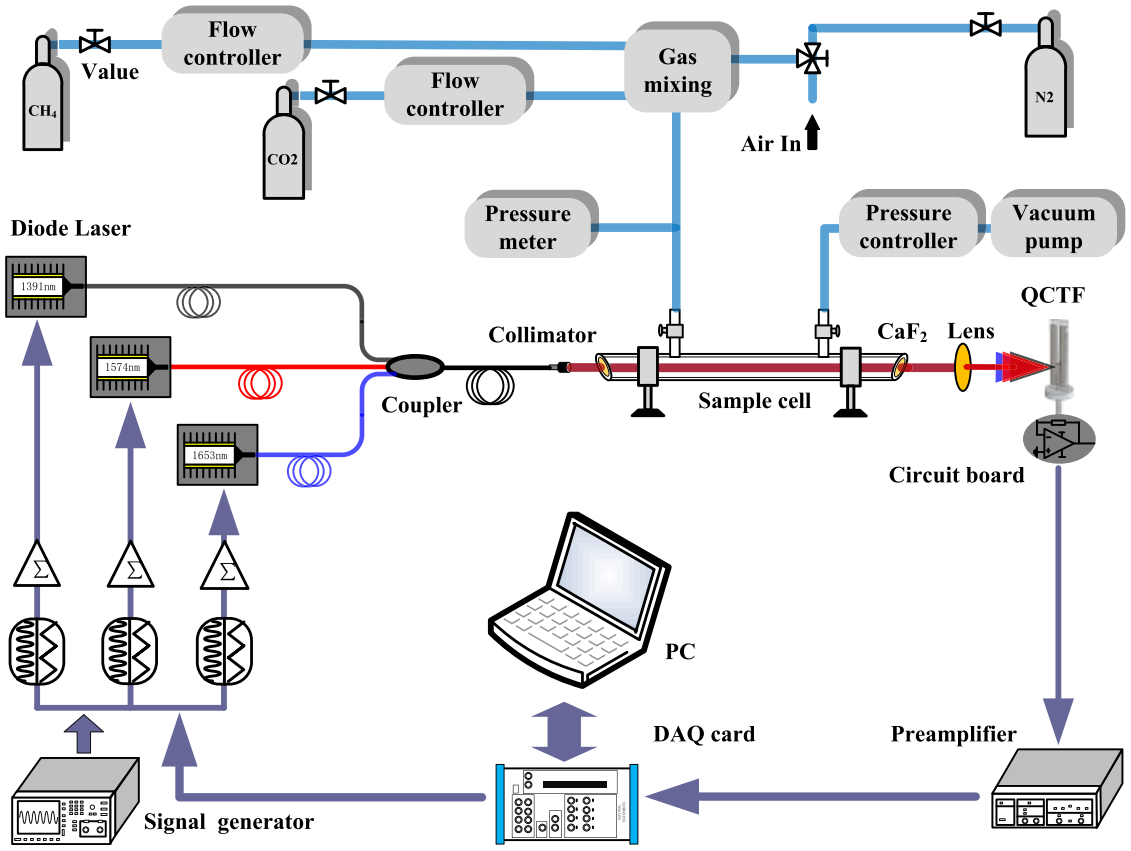

Figure 4. Schematic configuration of the multigas sensor system.

and resonant effects to realize photoelectric signal conversion. Unlike QEPAS, the incoming laser directly strikes on the surface of the tuning fork. For signal processing, a home-made circuit with a feedback resistor of 10 MΩ was applied to transform the piezoelectric current generated by the QCTF into a voltage signal and then further amplified by a low-noise preamplifier (SR560, Stanford Research Systems). The signal was acquired using a data acquisition (DAQ) card (NI USB-6259, 1.25 MHz sampling rate), which was based on a LabVIEW program. To achieve WMS detection, three signal adders are used to superimpose low-frequency laser scanning voltage and high-frequency modulation voltage signals, which are generated from the DAQ card and signal generator (AFG1022 Tektronix), respectively. Three superimposed voltage signals were finally used to drive the three lasers. Standard gas samples with different concentrations are prepared with a gas handling system, which mainly comprises some needle valves and connectors, a pressure controller (PC3-Series ALICAT), two flow controllers (MCR-2000 slpm ALICAT), and an air pump. The gas pressure is monitored using a digital gauge (Testo 552, Germany).

RESULTS AND DISCUSSION

Tri-frequency Modulation Technology. The resonance frequency properties of the QCTF should be exactly acquired before the actual application. A near-infrared diode laser at 1550 nm was used as the excitation light source for testing the resonant profile of the QCTF. The frequency response curve was recorded at one atmospheric pressure and the theoretically calculated profile based on a Lorentzian function, is shown in Figure 5. From this figure, a central resonance frequency of f_0 = 32781.73 Hz at ambient pressure and a quality factor Q of 8335 were obtained. Typically, the resonance bandwidth of the QCTF is approximately 5 Hz. The quality factor Q value was calculated as the ratio of the central resonance frequency f_0 to the frequency bandwidth Δf at one-half of the square root of the signal maximum, which represents the signal enhancement factor. In theory, the QCTF can be used as an effective acoustic transducer or photoelectric detector, as long as the modulation frequency of the excited signal is within its

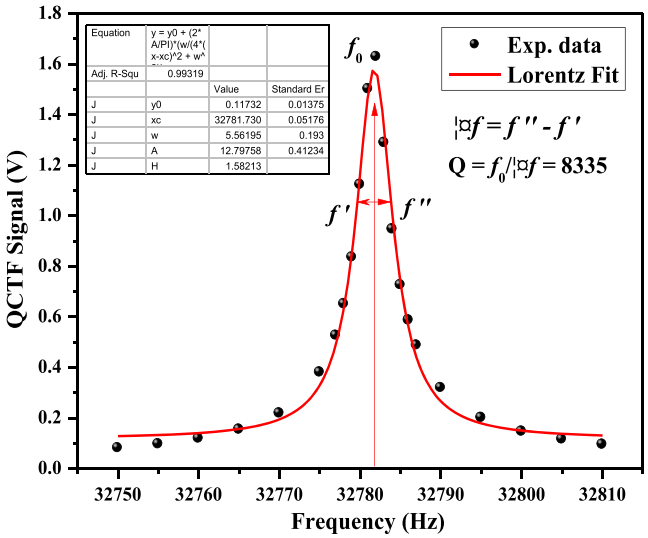

Figure 5. Experimentally measured resonant profile of the QCTF at ambient air and the fitted curve with a Lorentzian distribution, the acquired curve yielded Q = 8335.

https://dx.doi.org/10.1021/acs.analchem.0c03233
Anal. Chem. 2020, 92, 14153−14163

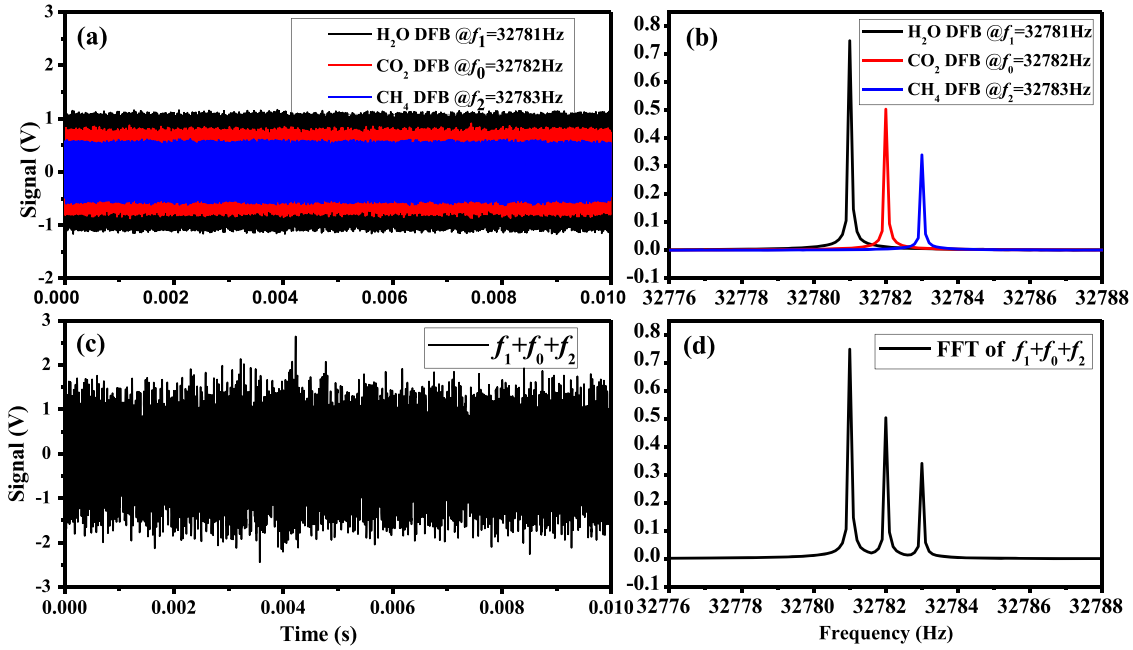

Figure 6. (a, b) QCTF signals of the time domain and corresponding frequency spectra solely excited by individual DFB diode lasers. (c, d) Time-domain signal and frequency-domain signal of the QCTF measured when the three lasers are simultaneously excited.

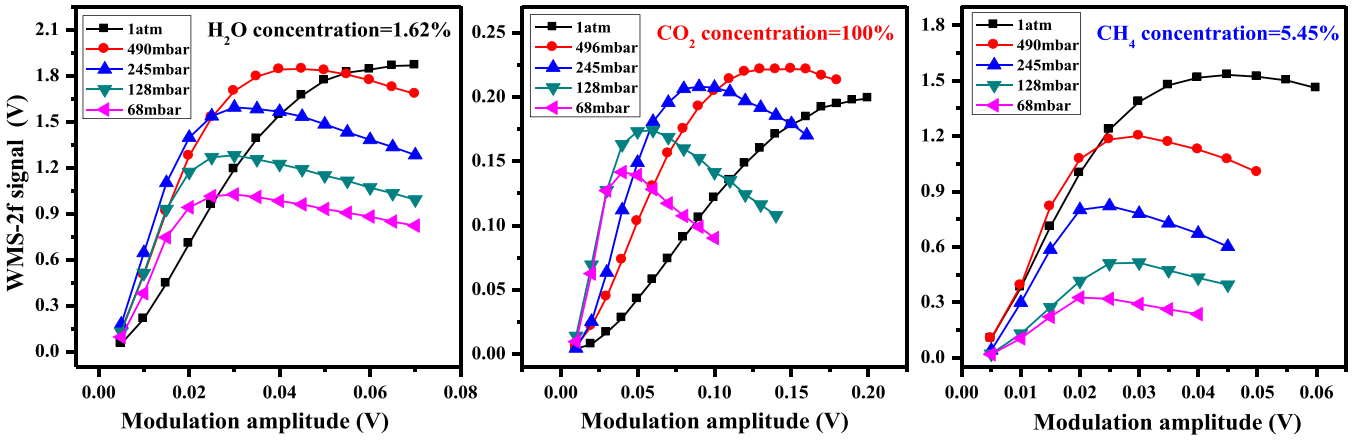

Figure 7. WMS-2*f* signal amplitudes as a function of the laser modulation amplitude at different pressures.

bandwidth. Obviously, the closer the modulation frequency f to the optimal center frequency f_0, the better the resonance effect. According to this idea, a multifrequency simultaneous modulation can be realized, if the relative electronics have enough precision. As for signal processing, individual frequency signals can be easily extracted using the powerful fast Fourier transform (FFT) algorithm.

With the limitation of experimental conditions, a tri-frequency modulation detection strategy is demonstrated in this article. Taking the resonance loss into account, a 1 Hz frequency interval near the optimal central resonance frequency f_0 was selected, i.e., $f_1 = f_0 - 1$ and $f_2 = f_0 + 1$. Finally, the DFB diode laser for H_2O with a fixed emitting wavelength at 1391.67 nm was modulated at f_1 = 32781 Hz, the DFB diode laser for CO_2 at 1574.03 nm was modulated at f_0 = 32782 Hz, and the DFB diode laser for CH_4 at 1653.72 nm was modulated at f_2 = 32783 Hz. The modulation amplitudes of the three DFB lasers were fixed at 20 mV. For example, Figure 6a,b shows the experimentally measured QCTF signals in the time domain and the corresponding frequency spectra are solely excited by the individual DFB diode laser. Correspondingly, the measured individual laser optical power is 14.9, 6.93, and 2.52 mW, respectively. Figure 6c,d shows the time-domain signal and the frequency-domain signal measured when the three lasers excite the QCTF simultaneously. In this case, the measured total laser optical power from the three integrated laser beams is about 24 mW, which agrees well with the sum of the three laser powers. As can be seen, the independent modulation signal is completely indistinguishable in the time domain, but they can be easily distinguished in the frequency domain after FFT signal processing. Note that the FFT peak amplitudes are almost the same in both cases, and the peak intensity has a significant dependence on the incident laser power (see details in the next section). The results prove that the tri-frequency or more frequency modulation is completely feasible for multigas detection simultaneously.

Optimization of the Wavelength Modulation. As we all know, the sensitive WMS-2*f* detection method is an indirect spectroscopy method, in which optimization of the modulation

https://dx.doi.org/10.1021/acs.analchem.0c03233
Anal. Chem. 2020, 92, 14153−14163

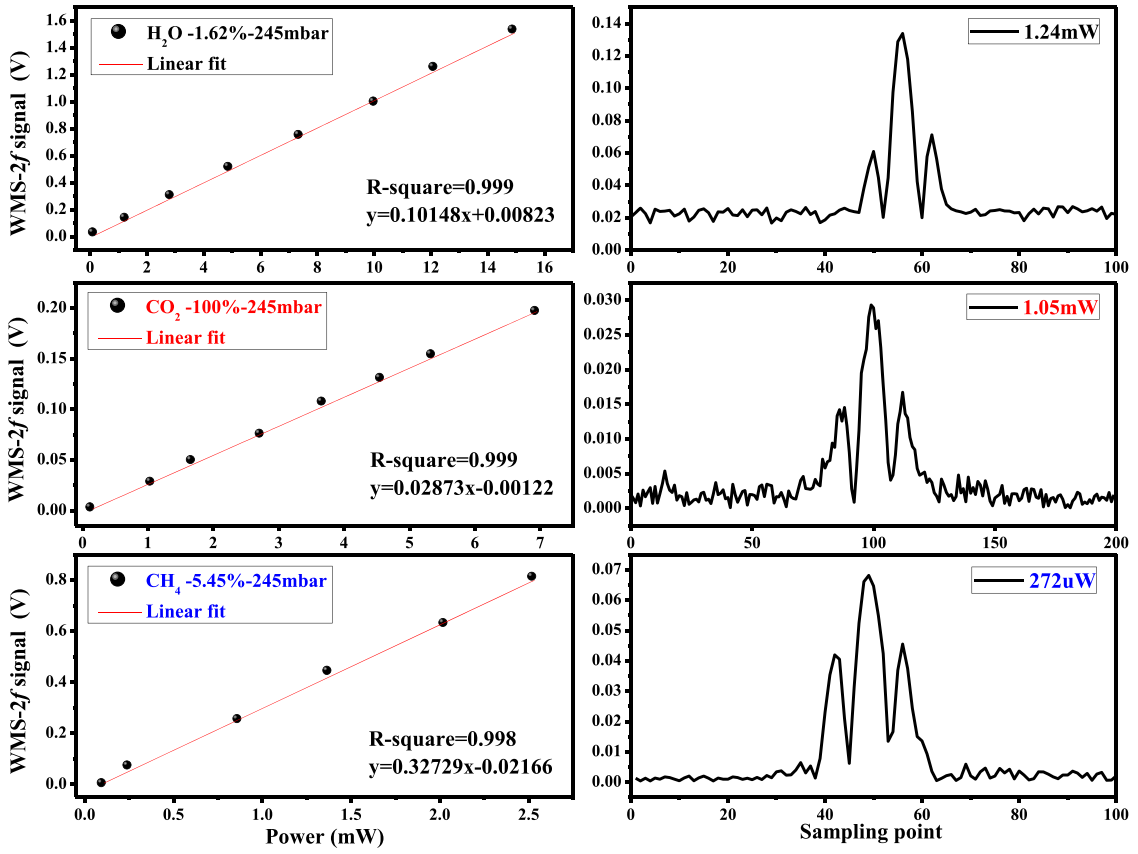

Figure 8. WMS-2*f* signal amplitude as a function of laser power (left panel) and WMS-2*f* spectra at a low power (right panel).

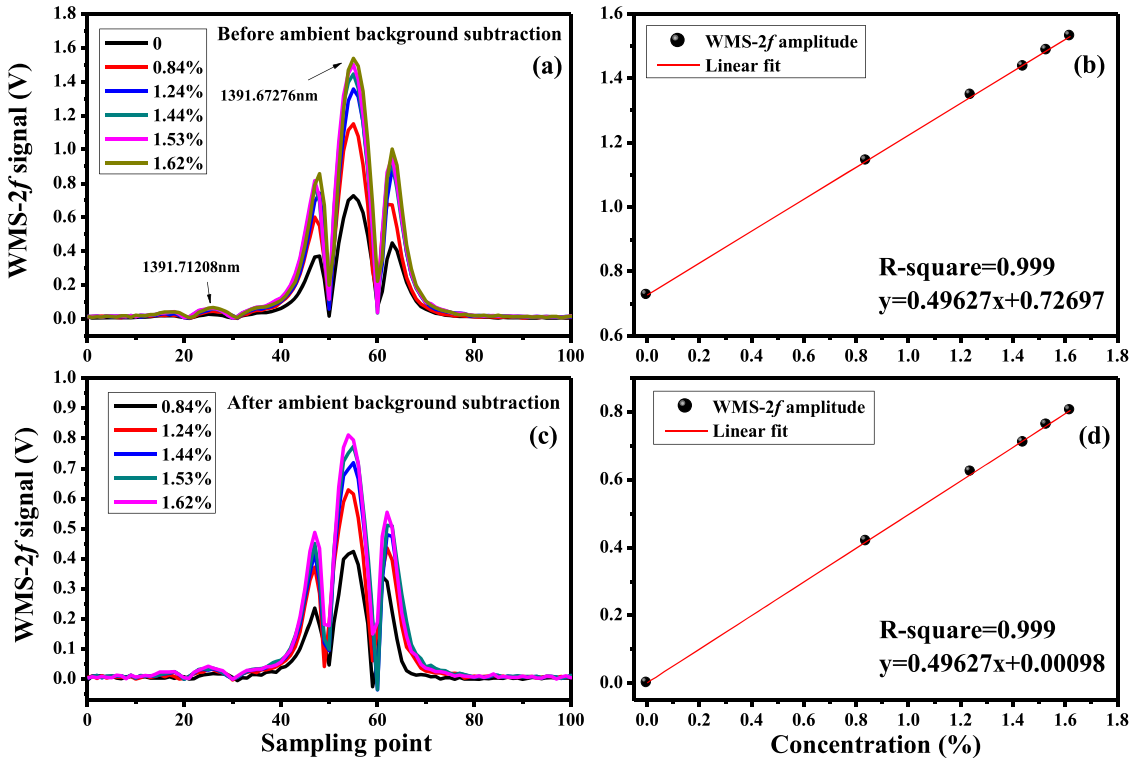

Figure 9. (a, b) WMS-2*f* absorption spectra before ambient background subtraction under different H_2O mixing ratios and the signal amplitude as a function of H_2O gas concentration. (c, d) WMS-2*f* absorption spectra after ambient background subtraction under different H_2O mixing ratios and the signal amplitude as a function of H_2O gas concentration.

https://dx.doi.org/10.1021/acs.analchem.0c03233
Anal. Chem. 2020, 92, 14153−14163

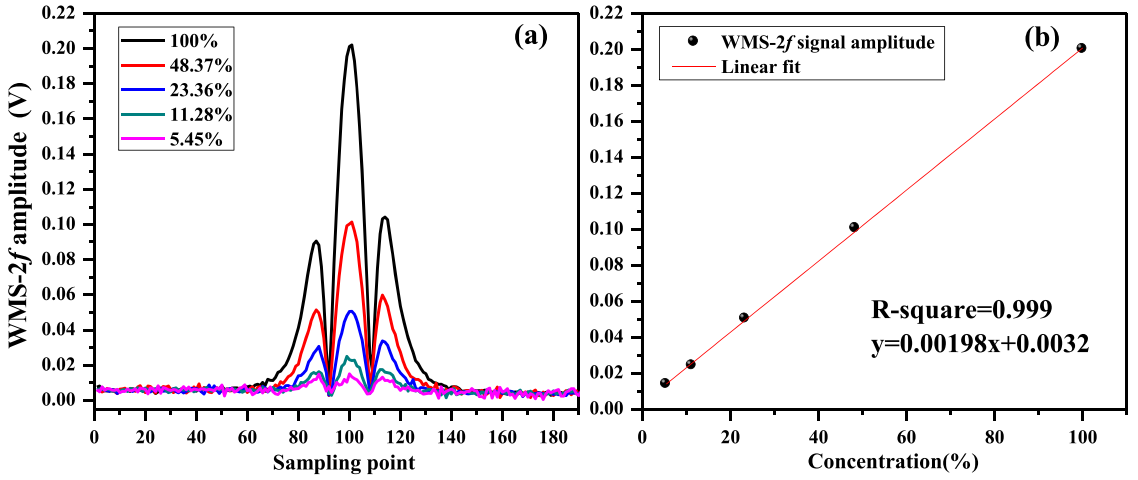

Figure 10. (a) WMS-2*f* absorption spectra under different CO_2 mixing ratios. (b) WMS-2*f* signal amplitude as a function of CO_2 gas concentration.

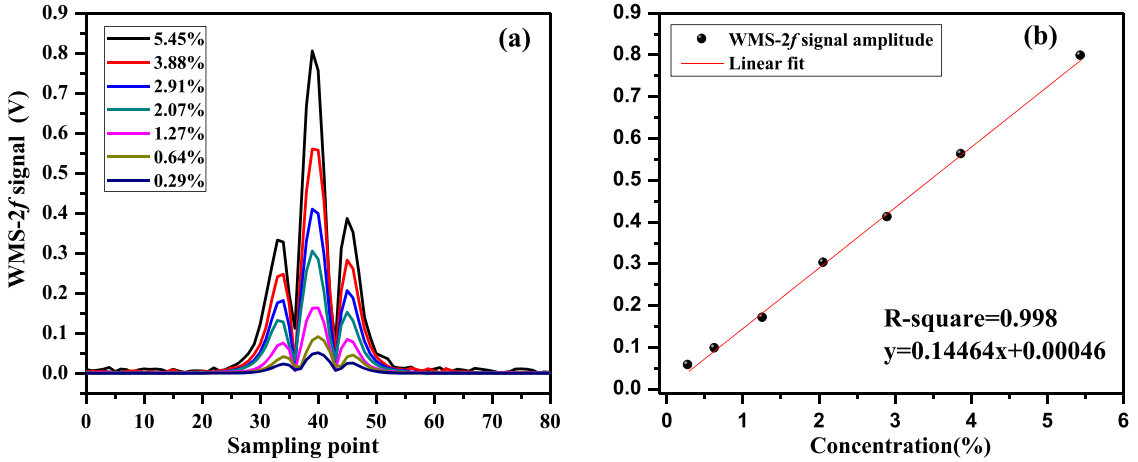

Figure 11. (a) WMS-2*f* absorption spectra under different CH_4 mixing ratios. (b) WMS-2*f* signal amplitude as a function of CH_4 gas concentration.

amplitude and gas sampling pressure and concentration of the linear calibration are necessary procedures before it can be used for gas concentration measurement. In the case of the QCTF-based WMS-2*f* detection scheme, we have to consider the resonant properties of the QCTF. Unlike the traditional single-frequency modulation, the modulation frequencies for the H_2O DFB laser, CO_2 DFB laser, and CH_4 DFB laser are selected as $f_1/2$ = 16390.5 Hz, $f_0/2$ = 16391.0 Hz, and $f_2/2$ = 16391.5 Hz, respectively, for realizing the tri-frequency modulation detection strategy. Figure 7 shows the measured WMS-2*f* signal amplitudes as a function of the laser modulation amplitude (in voltage) at different gas sample pressures for 1.62% H_2O, 100% CO_2, and 5.45% CH_4. Due to the molecular pressure broadening effect and the potential influence of the adjacent cross-sectional absorption interference, an optimum sampling pressure of 245 mbar was finally selected for the present sensor system. Correspondingly, the optimal modulation amplitudes for H_2O, CO_2, and CH_4 are 0.025, 0.07, and 0.02 V, respectively.

Moreover, the photon-to-electron conversion efficiency of the QCTF shows a significant dependence on the incident laser power, as demonstrated above. Therefore, the response characteristics of the QCTF on the three DFB diode lasers emitting power were investigated here. Experimentally, the laser emission wavelength of the three DFB diode lasers was always fixed at the corresponding molecular absorption line positions. The maximum output power is initially used and then is reduced step by step through an optical fiber attenuator. Figure 8 (left panel) presents the relationship between the output laser power and WMS-2*f* signal amplitude with the three gas samples of 1.62% H_2O, 100% CO_2, and 5.45% CH_4, respectively. The experimental results were measured with each laser operating independently at the optimal pressure of 245 mbar and the optimal modulation amplitudes mentioned above. For example, WMS-2*f* absorption spectra recorded in wavelength scanning mode are presented under the conditions of a low laser power, as shown in Figure 8 (right panel). The results indicate that the QCTF detector has a good linear response on the incident laser power, and the detectable optical power of the μW level can be easily achieved.

Linear Calibration. Under the optimum experimental conditions (i.e., sample pressure and modulation amplitude), the characteristics of the sensor system on the gas concentration response was further investigated. As for H_2O samples, laboratory indoor air was used and diluted with high purity dry nitrogen (N_2). The result measured by the hygrometer indicates that the laboratory temperature of 25 °C is almost constant and the relative humidity is 50.2% during the whole experiment. Combining with the saturated vapor pressure (31.6768 mbar) of H_2O at 25 °C, we can obtain the initial H_2O concentration of indoor air of about 1.62%. Figure

https://dx.doi.org/10.1021/acs.analchem.0c03233
Anal. Chem. 2020, 92, 14153−14163

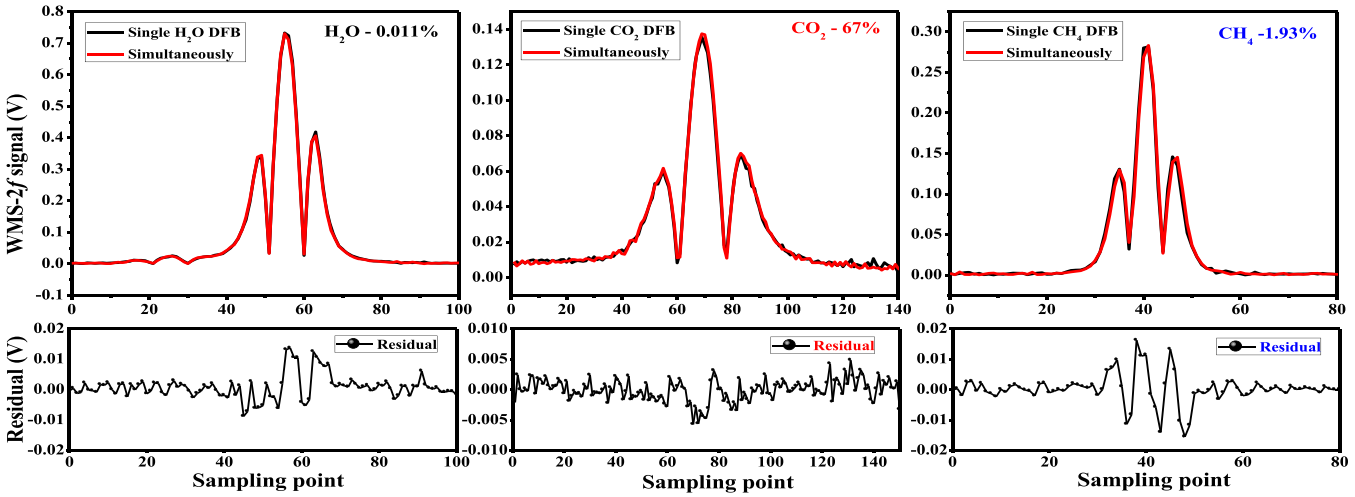

Figure 12. Comparison of the single measurement from the traditional individual modulation and the simultaneous measurement from the tri-frequency modulation.

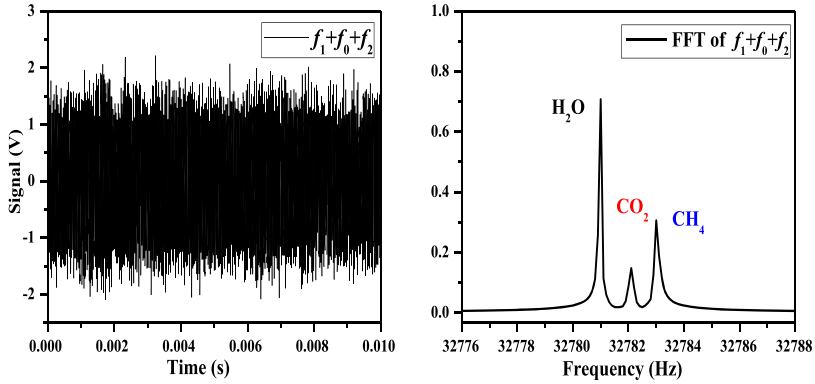

Figure 13. Time-domain signal and frequency-domain signal of the WMS-2*f* amplitude measured when the three lasers were simultaneously excited under sample concentrations of 0.011% H_2O, 67% CO_2, and 1.93% CH_4.

9a shows the measured WMS-2*f* signal of H_2O near 1391.67 nm with H_2O mixing ratios between 0 and 1.62%, and the calibration linear curve between the WMS-2*f* signal amplitude and H_2O concentration is plotted in Figure 9b. As can be seen in this figure, a weaker absorption peak located at 1391.71 nm within the laser scanning range is also observed. Considering the environmental effect, such as ambient air absorption from outside gas sample cell (an optical path of ~12 cm) and the potential residual water vapor in a N_2 cylinder, the WMS-2*f* spectrum recorded under the high purity dry N_2 was used as a background signal and subtracted from all of the diluted H_2O sample signals. After ambient background subtraction, the relative results are depicted in Figure 9c,d. All of the results show that the sensor system has a good linear response on the H_2O concentration with a regression coefficient R^2 of 0.999. In the case of the CO_2 and CH_4 calibration process, two separate gas cylinders of CO_2 and CH_4 were used and diluted with N_2 using a similar procedure, but the background subtraction is not done, as CO_2 and CH_4 absorption in ambient air is completely negligible. Finally, the measured WMS-2*f* signals of CO_2 and CH_4 at different concentrations and the relationship between the signal amplitude and concentration are presented in Figures 10 and 11, respectively. Both results show a good linear response too, with a regression coefficient R^2 of 0.999 (for CO_2) and 0.998 (for CH_4).

Simultaneous Detection with Tri-Frequency Modulation. The tri-frequency modulation detection scheme was finally evaluated for simultaneous detection of H_2O, CO_2, and CH_4 and compared with traditional individual modulation detection. A gas mixture sample of H_2O, CO_2, and CH_4 with concentrations of 0.011, 67, and 1.93%, respectively, were prepared in the gas cell. For individual modulation detection, only one laser is coupled into the 3 × 1 fiber coupler, the other two lasers are not coupled into the beam path. For instance, spectral signals of H_2O, CO_2, and CH_4 with different modulation schemes are shown in Figure 12, for comparison, the corresponding residual (i.e., tri-frequency modulation minus individual modulation detection) is also presented below. It can be seen from the figure that the measured WMS-2*f* signals have good consistency. The slight difference in the absorption center is possibly attributed to the instability of the laser wavelength, since all of the absorption spectra are recorded in a single laser scan.

The stability and accuracy of the sensor system are further evaluated by the continuous measurement of the constant mixture gas sample. In this case, each laser operates at a fixed wavelength mode, namely corresponding to the maximum value of the WMS-2*f* signal. Figure 13 demonstrates the original time-domain signal recorded in the tri-frequency modulation mode and the corresponding frequency-domain signal after FFT algorithm processing. Comparing with Figure

https://dx.doi.org/10.1021/acs.analchem.0c03233
Anal. Chem. 2020, 92, 14153−14163

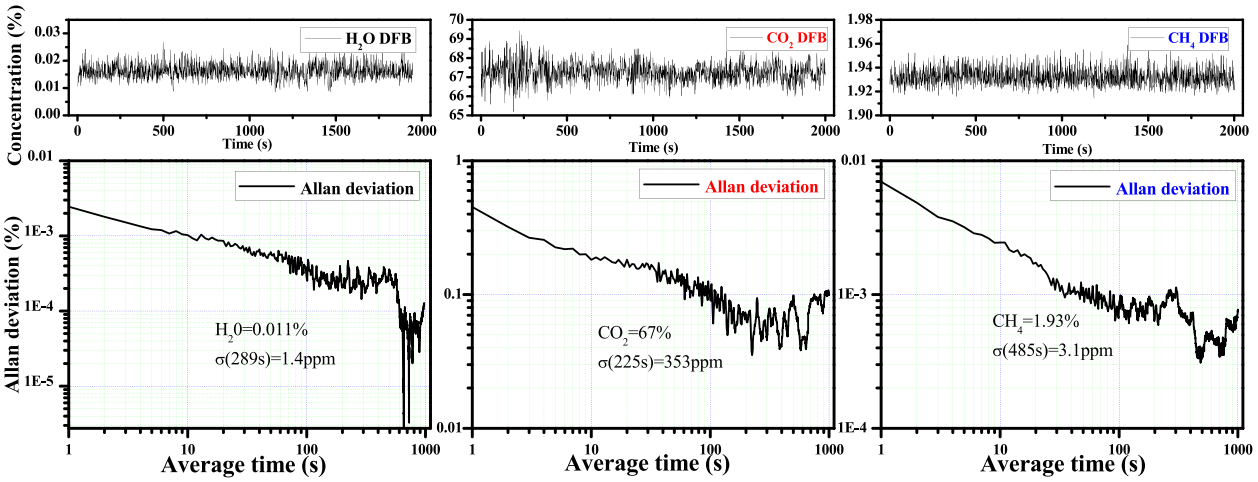

Figure 14. Allan-Werle deviation as a function of the signal averaging time measured by tri-frequency modulation detection.

6, the obvious variation of the FFT peak amplitude is correlated with gas molecule absorption. Thus, the higher the molecule absorption, the lower the transmitted light intensity after the gas cell; the lower the transmitted light intensity, the smaller the FFT peak value. The change of the FFT peak amplitude with and without molecule absorption can be directly converted into a concentration value based on the calibration curve. A continuous observation with more than 30 min was made, as shown in Figure 14, and the Allan-Werle deviation analysis was performed. The Allan-Werle deviation plot indicates that a measurement precisions of 1.4 ppm for H_2O @1391.67 nm, 353 ppm for CO_2 @1574.03 nm, and 3.1 ppm for CH_4 @1653.72 nm were achieved with 289, 225, and 485 s of integration time, respectively. The corresponding normalized noise equivalent absorption (NNEA) coefficients were calculated to be 2.65×10^{-10} $cm^{-1}W/\sqrt{Hz}$ for H_2O, 8.09×10^{-10} $cm^{-1}W/\sqrt{Hz}$ for CO_2, and 8.28×10^{-10} $cm^{-1}W/\sqrt{Hz}$ for CH_4, for the multigas sensor. Although the absolute sensitivity is not the greatest concern in this work, a simple comparison with similar gas sensor systems involving less than three molecule detection schemes are made and summarized in Table 2. Note that the detection limit of H_2S molecules reported in this work is estimated by combining the line intensity ratio of the selected transition line with CO_2 experimental results. From this comparison, we can conclude that the proposed multifrequency modulation detection scheme has a comparable sensitivity (even a slightly better performance for a particular species) than the traditional single-frequency modulation mode. However, the proposed trace gas sensor strategy has great advantages in developing ultraportable, multifunctional gas sensors and commercial value.

Table 2. Comparison of the Sensitivity Achieved with Previous Publications

species	wavelength (μm)	power (mW)	sensitivity (ppm)	NNEA ($cm^{-1}W/\sqrt{Hz}$)	ref
H_2S	1.58	38.3	9.1	5.3×10^{-9}	41
CO_2	1.58	37.9	123	4.0×10^{-9}	
CH_4	1.65	16.0	0.5	3.7×10^{-9}	
CH_4	1.653	11	79		42
H_2O	1.369		1.3		
C_2H_2	1.53	12	5		
C_2H_2	1.532	12	1		43
CH_4	1.653	11	13.14		
H_2O	1.391	14.9	1.4	2.65×10^{-10}	this
CO_2	1.574	6.93	353	8.09×10^{-10}	work
H_2S	1.573	6.93	92		
CH_4	1.653	2.52	3.1	8.28×10^{-10}	

EDFA Used for Improving Sensitivity. Note that the selected line strength of the CO_2 molecule is very weak, so that the spectral signal-to-noise ratio (SNR) at low concentrations is relatively poor, which is the major factor that limits the detection limit of CO_2. The method of using an erbium-doped fiber amplifier (EDFA) to increase the output power of the laser has been proved as a highly effective approach in PAS or QEPAS detection techniques.[44,45] According to the power dependence of the QCTF detector, a home-made EDFA with a maximum amplification power of 35 mW (laser output) was used for improving CO_2 sensitivity. By combining the EDFA with the DFB laser for the CO_2 molecule, an effective laser power between 0 to 17.25 mW was measured before the QCTF. Figure 15a shows the WMS-2*f* spectrum of the pure CO_2 sample at different laser powers (measured before the QCTF). Figure 15b shows the relationship between the WMS-2*f* signal amplitude and laser power. We found that signal amplification is accompanied by the introduction of additional noise. Linear fitting between the WMS-2*f* signal amplitude and laser power yields a good linearity relationship with a regression coefficient R^2 of 0.992 and 0.993, respectively, for the original amplification signal and background subtraction signal. The trend of the noise level and SNR values versus optical power is depicted in Figure 16. The noise level and SNR values show an increasing trend within this EDFA power range. To evaluate the effect of sensitivity enhancement, the sample gas cell was evacuated and filled with 5.95% CO_2 to analyze the WMS-2*f* signals. Figure 17 shows the comparison of WMS-2*f* spectra with and without using an EDFA. According to the usual noise statistical method as labeled with a rectangular box, the calculated noise levels (1σ) are 0.00127 and 0.00622, corresponding to the SNR of 11 and 23, respectively. As theory expected, the SNR (i.e., sensitivity) has been improved by 2 times using an EDFA. We believe that the sensitivity enhancement effect will be more significant, if a higher magnification EDFA is available.

https://dx.doi.org/10.1021/acs.analchem.0c03233
Anal. Chem. 2020, 92, 14153−14163

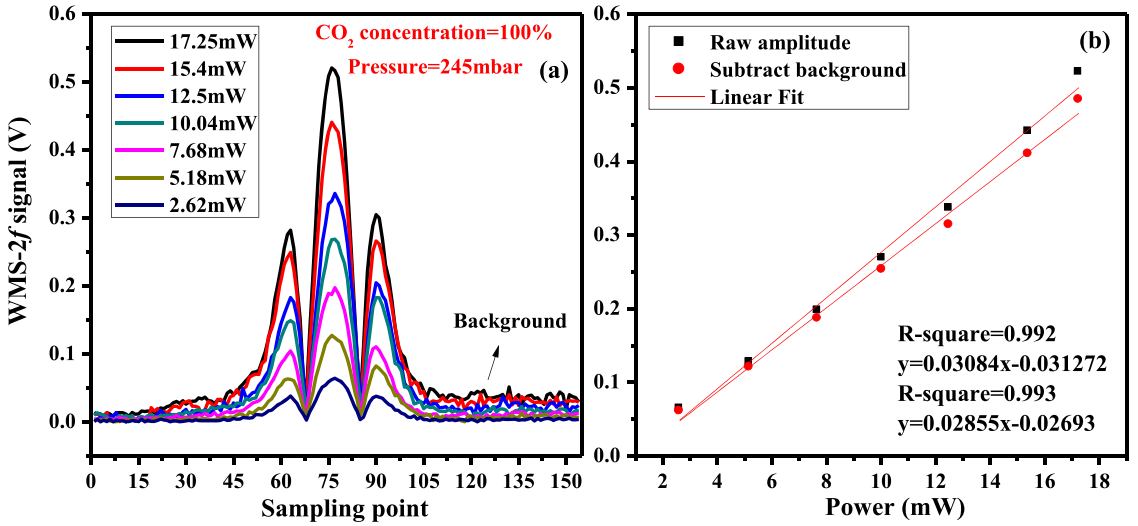

Figure 15. (a) WMS-2*f* spectrum of 100% CO_2 at different laser powers. (b) WMS-2*f* signal amplitude as a function of laser power.

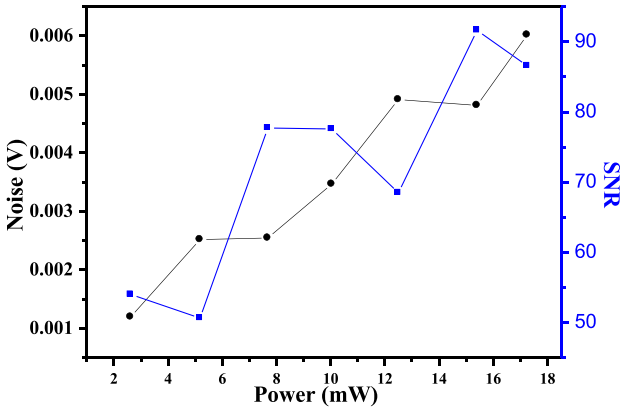

Figure 16. WMS-2*f* signal noise level and SNR value versus laser power.

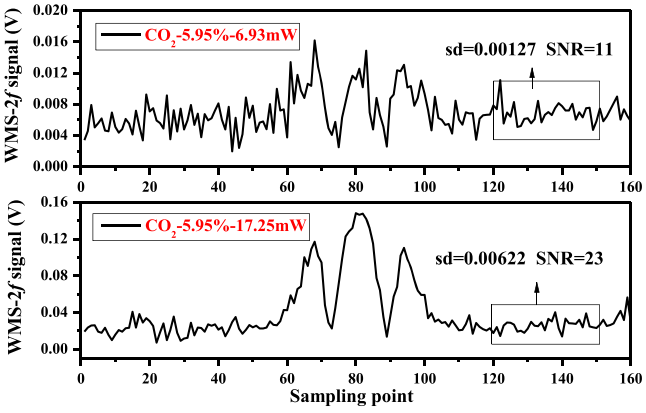

Figure 17. WMS-2*f* spectra of 5.95% CO_2 and the comparison with and without using an EDFA.

CONCLUSIONS

In conclusion, we reported a multigas detection system based on a single QCTF and tri-frequency modulation technology, which has been successfully demonstrated for synchronous detection of H_2O, CO_2, and CH_4 using three different near-infrared DFB diode lasers. Tunable diode laser wavelength modulation spectroscopy was used for enhancing detection sensitivity. The results indicate that the detection limits of 1.4, 353, and 3.1 ppm for H_2O, CO_2 and CH_4, respectively, can be obtained. Corresponding to the normalized noise equivalent absorption (NNEA) coefficients of 2.65×10^{-10}, 8.09×10^{-10}, and 8.28×10^{-10} cm^{-1} W/$\sqrt{Hz}$, which are comparable (even slightly better for a particular species) than the traditional single-frequency modulation mode. The sensitivity can be further improved using an EDFA to achieve a high laser power. Most importantly, the proposed sensor architecture has the significant advantages of an easier optical alignment, lower cost, and developing ultraportable, multifunctional gas sensors compared with a conventional TDLAS sensor based on multiple photoelectric detectors. Note that this technique can also be extended to other wavelength ranges for other species of interest, and the popular QEPAS technique with the QCTF as an acoustic transducer.

AUTHOR INFORMATION

Corresponding Author

Jingsong Li − *Laser Spectroscopy and Sensing Laboratory, Anhui University, 230601 Hefei, China; State Key Laboratory of Applied Optics, Changchun Institute of Optics, Fine Mechanics and Physics, Chinese Academy of Sciences, Changchun 130033, China;* orcid.org/0000-0002-6872-465X; Phone: +86-551-63861490; Email: ljs0625@126.com

Authors

Linguang Xu − *Laser Spectroscopy and Sensing Laboratory, Anhui University, 230601 Hefei, China*

Sheng Zhou − *Laser Spectroscopy and Sensing Laboratory, Anhui University, 230601 Hefei, China*

Ningwu Liu − *Laser Spectroscopy and Sensing Laboratory, Anhui University, 230601 Hefei, China*

Minghui Zhang − *Laser Spectroscopy and Sensing Laboratory, Anhui University, 230601 Hefei, China*

Jingqiu Liang − *State Key Laboratory of Applied Optics, Changchun Institute of Optics, Fine Mechanics and Physics, Chinese Academy of Sciences, Changchun 130033, China*

Complete contact information is available at: https://pubs.acs.org/10.1021/acs.analchem.0c03233

https://dx.doi.org/10.1021/acs.analchem.0c03233
Anal. Chem. 2020, 92, 14153−14163

Author Contributions

All authors have given approval to the final version of the manuscript.

Notes

The authors declare no competing financial interest.

■ ACKNOWLEDGMENTS

The authors gratefully acknowledge the financial support from the National Program on Key Research and Development Project (2016YFC0302202), the National Natural Science Foundation of China (41875158, 61675005, 61627819, 61727818 , 61905001), the Strategic Priority Research Program of the Chinese Academy of Sciences (XDA17040513) and the Open Fund of State Key Laboratory of Applied Optics (SKLAO2020001A13).

■ REFERENCES

(1) Liu, K.; Wang, L.; Tan, T.; Wang, G. S.; Zhang, W. J.; Chen, W. D.; Gao, X. M. *Sens. Actuators, B* **2015**, *220*, 1000−1005.
(2) Sun, H. Y.; Ma, Y. F.; He, Y.; Qiao, S.; Yang, X. T.; Tittel, F. K. *Infrared Phys. Technol.* **2019**, *102*, No. 103012.
(3) Ma, Y. F. *Appl. Sci.* **2018**, *8*, No. 1822.
(4) Li, Y.; Wang, R. Z.; Tittel, F. K.; Ma, Y. F. *Opt. Lasers Eng.* **2020**, *132*, No. 106155.
(5) Li, J. S.; Chen, W. D.; Fischer, H. *Appl. Spectrosc. Rev.* **2013**, *48*, 523−559.
(6) Hodgkinson, J.; Tatam, R. P. *Meas. Sci. Technol.* **2013**, *24*, No. 012004.
(7) McCurdy, M. R.; Bakhirkin, Y.; Wysocki, G.; Lewicki, R.; Tittel, F. K. *J. Breath Res.* **2007**, *1*, No. 014001.
(8) Schwaighofer, A.; Brandstetter, M.; Lendl, B. *Chem. Soc. Rev.* **2017**, *46*, 5903−5924.
(9) Kosterev, A. A.; Bakhirkin, Y. A.; Curl, R. F.; Tittel, F. K. *Opt. Lett.* **2002**, *27*, No. 1902.
(10) Zheng, H.; Yin, X.; Dong, L.; Wu, H.; Liu, X.; Ma, W.; Zhang, L.; Yin, W.; Jia, S. *J. Spectrosc.* **2015**, *2015*, No. 218413.
(11) Liu, K.; Guo, X.; Yi, H.; Chen, W.; Zhang, W.; Gao, X. *Opt. Lett.* **2009**, *34*, 1594−1596.
(12) Patimisco, P.; Sampaolo, A.; Zheng, H.; Dong, L.; Tittel, F. K.; Spagnolo, V. *Adv. Phys.: X* **2017**, *2*, 169−187.
(13) Li, S. Z.; Dong, L.; Wu, H. P.; Sampaolo, A.; Patimisco, P.; Spagnolo, V.; Tittel, F. K. *Anal. Chem.* **2019**, *91*, 5834−5840.
(14) Van Neste, C. W.; Senesac, L. R.; Thundat, T. *Appl. Phys. Lett.* **2008**, *92*, No. 234102.
(15) Liu, N. W.; Zhou, S.; Zhang, L.; Yu, B. L.; Fischer, H.; Ren, W.; Li, J. S. *Laser Phys. Lett.* **2018**, *15*, No. 085701.
(16) Sun, J.; Deng, H.; Liu, N. W.; Wang, H.; Yu, B. L.; Li, J. S. *Rev. Sci. Instrum.* **2016**, *87*, No. 123101.
(17) Ma, Y. F.; He, Y.; Tong, Y.; Yu, X.; Tittle, F. K. *Opt. Express* **2018**, *26*, 32103−32110.
(18) Ma, Y.; He, Y.; Patimisco, P.; Sampaolo, A.; Qiao, S.; Yu, X.; Tittel, F. K.; Spagnolo, V. *Appl. Phys. Lett.* **2020**, *116*, No. 011103.
(19) Patimisco, P.; Sampaolo, A.; Dong, L.; Tittel, F. K.; Spagnolo, V. *Appl. Phys. Rev.* **2018**, *5*, No. 011106.
(20) Friedt, J. M.; Carry, É. *Am. J. Phys.* **2007**, *75*, 415−422.
(21) Elefante, A.; Giglio, M.; Sampaolo, A.; Menduni, G.; Patimisco, P.; Passaro, V. M. N.; Wu, H. P.; Rossmadl, H.; Mackowiak, V.; Cable, A.; Tittel, F. K.; Dong, L.; Spagnolo, V. *Anal. Chem.* **2019**, *91*, 12866−12873.
(22) Li, J. S.; Reiffs, A.; Parchatka, U.; Fischer, H. *Metrol. Meas. Syst.* **2015**, *22*, 25−38.
(23) Wang, C.; Sahay, P. *Sensors* **2009**, *9*, 8230−8262.
(24) He, Y. B.; Kan, R. F.; Englich, F. V.; Liu, W. Q.; Orr, B. J. *Opt. Express* **2010**, *18*, 20059−20071.
(25) Sur, R.; Sun, K.; Jeffries, J. B.; Hanson, R. K. *Appl. Phys. B* **2014**, *115*, 9−24.
(26) Lewander, M.; Fried, A.; Weibring, P.; Richter, D.; Spuler, S.; Rippe, L. *Appl. Phys. B* **2011**, *104*, 715−723.
(27) Kühnreich, B.; Wagner, S.; Habig, J. C.; Möhler, O.; Saathoff, H.; Ebert, V. *Appl. Phys. B* **2015**, *119*, 177−187.
(28) Santoni, G. W.; Daube1, B. C.; Kort, E. A.; Jiménez, R.; Park, S.; Pittman, J. V.; Gottlieb1, E.; Xiang, B.; Zahniser, M. S.; Nelson, D. D.; McManus, J. B.; Peischl, J.; Ryerson, T. B.; Holloway, J. S.; Andrews, A. E.; Sweeney, C.; Hall, B.; Hintsa, E. J.; Moore, F. L.; Elkins, J. W.; Hurst, D. F.; Stephens, B. B.; Bent, J.; Wofsy, S. C. *Atmos. Meas. Tech.* **2014**, *7*, 1509−1526.
(29) Chen, X.; Yang, C. G.; Hu, M.; Shen, J. K.; Niu, E. C.; Xu, Z. Y.; Fan, X. L.; Wei, M.; Yao, L.; He, Y. B.; Liu, J. G.; Kan, R. F. *Chin. Phys. B* **2018**, *27*, No. 040701.
(30) Genner, A.; Martín-Mateos, P.; Moser, H.; Lendl, B. *Sensors* **2020**, *20*, No. 1850.
(31) Hugi, A.; Terazzi, R.; Bonetti, Y.; Wittmann, A.; Fischer, M.; Beck, M.; Faist, J.; Gini, E. *Appl. Phys. Lett.* **2009**, *95*, No. 061103.
(32) Yu, Y. J.; Sanchez, N. P.; Griffin, R. J.; Tittel, F. K. *Opt. Express* **2016**, *24*, 10391−10401.
(33) Weidmann, D.; Tsai, T.; Macleod, N. A.; Wysocki, G. *Opt. Lett.* **2011**, *36*, 1951−1953.
(34) Li, J. S.; Liu, N. W.; Ding, J. Y.; Zhou, S.; He, T. B.; Zhang, L. *Opt. Lasers Eng.* **2019**, *115*, 141−148.
(35) Rodhe, H. *Science* **1990**, *248*, 1217−1219.
(36) Nisbet, E. G.; Dlugokencky, E. J.; Bousquet, P. *Science* **2014**, *343*, 493−495.
(37) Dai, B.; Jones, C.; Pearl, M.; Pelletier, M.; Myrick, M. *Sensors* **2018**, *18*, No. 2006.
(38) Wu, H.; Dong, L.; Zheng, H.; Liu, X.; Yin, X.; Ma, W.; Zhang, L.; Yin, W.; Jia, S.; Tittel, F. K. *Sens. Actuators, B* **2015**, *221*, 666−672.
(39) Wu, H.; Sampaolo, A.; Dong, L.; Patimisco, P.; Liu, X.; Zheng, H.; Yin, X.; Ma, W.; Zhang, L.; Yin, W.; Spagnolo, V.; Jia, S.; Tittel, F. K. *Appl. Phys. Lett.* **2015**, *107*, No. 111104.
(40) Gordon, I. E.; Rothman, L. S.; Hill, C.; Kochanov, R. V.; Tan, Y.; Bernath, P. F.; Birk, M.; Boudon, V.; Campargue, A.; Chance, K. V.; Drouin, B. J.; Flaud, J. M.; Gamache, R. R.; Hodges, J. T.; Jacquemart, D.; Perevalov, V. I.; Perrin, A.; Shine, K. P.; Smith, M. A. H.; Tennyson, J.; Toon, G. C.; Tran, H.; Tyuterev, V. G.; Barbe, A.; Csaszar, A. G.; Devi, V. M.; Furtenbacher, T.; Harrison, J. J.; Hartmann, J. M.; Jolly, A.; Johnson, T. J.; Karman, T.; Kleiner, I.; Kyuberis, A. A.; Loos, J.; Lyulin, O. M.; Massie, S. T.; Mikhailenko, S. N.; Moazzen-Ahmadi, N.; Mueller, H. S. P.; Naumenko, O. V.; Nikitin, A. V.; Polyansky, O. L.; Rey, M.; Rotger, M.; Sharpe, S. W.; Sung, K.; Starikova, E.; Tashkun, S. A.; Auwera, J. V.; Wagner, G.; Wilzewski, J.; Wcislo, P.; Yu, S.; Zak, E. J. *J. Quant. Spectrosc. Radiat. Transfer* **2017**, *203*, 3−69.
(41) Kosterev, A. A.; Dong, L.; Thomazy, D.; Tittel, F. K.; Overby, S. *Appl. Phys. B* **2010**, *101*, 649−659.
(42) Zhang, Q.; Chang, J.; Cong, Z.; Sun, J.; Wang, Z. *IEEE Photonics J.* **2018**, *10*, 1−8.
(43) Wang, Z. L.; Chang, J.; Tian, C. W.; Feng, Y. W.; Wang, C.; Zhang, H.; Zhang, Q. D.; Li, H. F.; Feng, Z. B.; Zhang, X. K.; Tang, L. F. *Appl. Opt.* **2019**, *58*, 8479−8485.
(44) Wu, H. P.; Dong, L.; Zheng, H. D.; Liu, X. L.; Yin, X. K.; Ma, W. G.; Zhang, L.; Yin, W. B.; Jia, S. T.; Tittel, F. K. *Sens. Actuators, B* **2015**, *221*, 666−672.
(45) Ma, Y. F.; He, Y.; Zhang, L. G.; Yu, X.; Zhang, J. B.; Sun, R.; Tittel, F. K. *Appl. Phys. Lett.* **2017**, *110*, No. 031107.

https://dx.doi.org/10.1021/acs.analchem.0c03233
Anal. Chem. 2020, 92, 14153−14163